Journal Name

ARTICLE TYPE

Cite this: DOI: 10.1039/xxxxxxxxxx

Understanding the interplay between solvent and nuclear rearrangements in the negative solvatochromism of a push-pull flexible quinolinium cation †

Oliviero Cannelli,[a,b] Tommaso Giovannini,[a] Alberto Baiardi,[a] Benedetta Carlotti,[c] Fausto Elisei,[c] and Chiara Cappelli,*[a]

Received Date
Accepted Date

DOI: 10.1039/xxxxxxxxxx

www.rsc.org/journalname

A detailed computational characterization of the One-Photon Absorption spectrum of 2-((E)-2-[2,2']-bithiophenyl-5-yl-vinyl)-1-methyl-quinolinium cation in acetonitrile solution is presented. The main physico-chemical effects (solvation, vibronic progression) affecting the band position and shape are progressively introduced in the computational model, highlighting their relative role on the spectral profile. The reported results underline how an accurate reproduction of the experimental spectrum can only be obtained by going beyond oversimplified methods. Moreover, the deep interplay between solvent effects and nuclear rearrangements permits to explain the negative solvatochromism exhibited by hypsochromic molecules. This illustrates the potentialities of the computational investigation, which can shed light on the information hidden in experimental spectra.

Introduction

In the last two decades, the increasing availability of computational resources and theoretical tools has paved the way to their extensive application to chemical problems, thus defining new and complementary strategies with respect to experiments.
In this respect, one of the main interests of computational chemistry is the reliable reproduction of absorption and emission spectra, which remains challenging especially for systems of increasing dimension. Indeed, numerous studies have been devoted to the evaluation of the performance of electronic structure methods at reproducing Vertical Transition energies (VTs) [1–8] or the energy associated with the transition between zero-point-vibrational levels (0-0 transitions) [9–14]. Further refinements in the computational tools have also allowed to extend the boundaries of the theoretical predictions beyond absorption or emission maxima, as highlighted by recent publications [15–26].
A valuable feature of computational approaches is the possibility to separate and identify different contributions to the spectral bandshape. As a result, theoretical investigations permit to access the information hidden beyond broad, low-resolution, experimental UV-Vis spectra, even for large and flexible systems, thanks to the availability of novel and reliable approaches to deal with the presence of Large Amplitude Motions (LAMs) [27] developed by some of the present authors.
In order to show the maturity of such approaches, a particularly challenging chemical system has been chosen in the present investigation, i.e. 2-((E)-2-[2,2']-bithiophenyl-5-yl-vinyl)-1-methyl-quinolinium cation (**M1**) (see Fig. 1), which is a push-pull medium-to-large flexible compound strongly sensitive to the external environment.

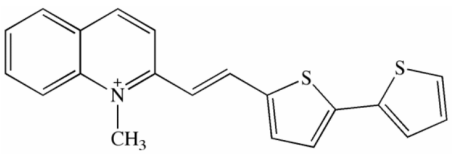

Fig. 1 2-((E)-2-[2,2']-bithiophenyl-5-yl-vinyl)-1-methyl-quinolinium cation chemical structure.

This system, whose experimental absorption spectrum exhibits an hypsochromic shift with the solvent polarity [28], belongs to a class of molecules of interest for their Non-Linear Optical (NLO) properties, deeply connected to the Intramolecular Charge Trans-

[a] *Scuola Normale Superiore, Piazza dei Cavalieri, 7, Pisa, Italy. Tel: +39 050 509263; E-mail: chiara.cappelli@sns.it*
[b] *Laboratoire de Spectroscopie Ultrarapide, ISIC-FSB, École Polytechnique Fédérale de Lausanne, CH 1015 Lausanne, Switzerland*
[c] *Department of Chemistry, Biology and Biotechnology and Centro di Eccellenza sui Materiali Innovativi Nanostrutturati (CEMIN), University of Perugia, via Elce di Sotto 8, 06123 Perugia, Italy.*
† Electronic Supplementary Information (ESI) available: details on DIA, BLA and CT indexes analysis. See DOI: 10.1039/b000000x/

fer (ICT) nature of the S_1 state. Moreover, its water solubility and antiproliferative properties, already demonstrated[29], make it promising for several NLO based technological applications[30–33]. Deep investigations on the spectral and kinetic properties of molecules bearing methylpyrydinium or methylquinolinium, positively charged, have been carried out by ultrafast time-resolved spectroscopy combined with quantum mechanical calculations[34–36]. In general, a negative (hypsochromic) solvatochromic effect on the absorption spectrum has been recorded and correlated with the change of dipole moment upon excitation.

The interesting features of **M1**, namely large dimensions, solvatochromism and flexibility (revealed experimentally[37] and theoretically[38] for a smaller compound as the dithiophene) make it difficult to be computationally studied. As it will be amply discussed in this work, the combination of refined computational tools permits to extract precious information enclosed in the experimental absorption spectrum, thus demonstrating the maturity and the potentialities of the computational investigation, which is becoming more and more a complementary and trustworthy approach to match with experimental investigations.

In the following, after a description of the employed protocol, the ground state of M1 is characterized. Then, the first excited state and One-Photon Absorption (OPA) spectra are studied, highlighting the role of different effects (vibronic progression, solvent) on spectral profiles and getting insight into the origin of the experimentally observed negative solvatochromism. Finally, computations and experiments are compared, showing remarkable accuracy as long as all the fundamental physical effects which influence the bandshape are included.

Experimental Section

The experimentally investigated compound 2-((E)-2-[2,2']-bithiophenyl-5-yl-vinyl)-1-methyl-quinolinium iodide was synthesized in the research group of Prof. C. G. Fortuna, University of Catania, following the procedure described in the literature[29]. Absorption measurements were performed in acetonitrile solvent, from Sigma Aldrich (spectrophotometric grade, used without purification), employing a PerkinElmer Lambda 800 spectrophotometer.

Computational Strategies

A full computational characterization of the OPA spectra is based on an accurate description of the Ground State (GS) and the Excited State (ES) using Quantum Mechanical (QM) approaches. Unfortunately, the dimension of large chemical systems prevents the application of computationally demanding wavefunction-based methods.

A valuable alternative is provided by Density Functional Theory (DFT), especially in its Kohn-Sham formulation, and Time-Dependent Density Functional Theory (TD-DFT), being the best compromise between accuracy and computational effort[19,24]. In this context, a suitable choice of the exchange-correlation functional is of crucial importance to get an accurate description of both GS and ES not only from a quantitative point of view, but also qualitatively[14,39–41].

The flexibility of non-rigid systems makes difficult the investigation of GS and ES. Indeed, it is required to identify GS stable structures accessible at room temperature and to carefully describe nuclear rearrangements following the electronic transition, and couple them with solvent effects.

A strong solvatochromism indirectly suggests a fundamental role of the solvent in the spectroscopic response. The most common strategy for describing the interaction between the environment and the molecule is to exploit QM/classical focused models, where the attention is centered on the solute, which is accurately modeled quantum-mechanically, whereas the solvent is described classically, at a lower level of sophistication. Several efficient QM/classical approaches to solvation phenomena exist, both keeping an atomistic, but classical description of the solvent (QM/MM approaches)[42–46] or smearing it out to a continuum[47]. Explicit QM/MM approaches outperform implicit continuum models whenever specific solute-solvent interactions play a leading role[44–46,48], especially when the mutual polarization of the MM and QM portions is taken into account. In case of non-protic solvents, an implicit description and in particular the Polarizable Continuum Model (PCM), have been widely demonstrated to give excellent results, at a computational cost comparable to that of the isolated systems[21,47,49].

In the PCM (employed in this work), the environment is modeled as an infinite, homogeneous, continuum, polarizable dielectric, and the solute molecule, described at QM level, is placed into a molecule-shaped cavity, surrounded by the continuum. The solute density induces a polarization density of charges on the cavity surface, which recursively modifies the density and the equilibrium geometry of the molecule.

During the measurement of molecular spectra of solvated systems, the charge density of the solute evolves in time as a result of the interaction with the incident radiation. Generally, the solvent cannot follow the evolution of the solute with all its degrees of freedom and, depending on the characteristic timescale of the external field, some of them remain static, entering a nonequilibrium configuration. In the case of UV-Vis absorption phenomena[50,51] the solvent can only respond with its electronic degrees of freedom (frequency-dependent dielectric constant), while the vibrational, rotational, and translational ones remain static (static dielectric constant of the solvent). Such a computational strategy has been accurately described in the literature[47] and has been successfully applied to the modeling of different electronic spectral properties[8,24,51].

For large and flexible system, one of the most interesting aspect of solvent models is their ability to take into account both modifications of the solute wavefunction ("direct effect") and nuclear equilibrium positions ("indirect effect"), which strongly influence the absorption spectrum.

However, the complete reproduction of absorption bandshapes requires to couple reliable solvation approaches and vibronic models[38,52–55], that can be efficiently extended to large systems in a feasible manner only working under the harmonic approximation. Two parallel vibronic approaches has been used in this work, namely the Time-Independent (TI) and the Time-Dependent (TD). Within the TI model, the final spectrum is ob-

tained as the sum of all the transitions between the vibrational initial and final states, treated independently of each another[38,56]. However, the number of transitions giving a non-negligible contribution to the overall spectrum is usually high, especially by including temperature effects and when dealing with large and flexible systems, as that studied in this work. These limitations can be overcome within the alternative TD approach, based on Feynmann path integral formalism[57,58], where the spectrum is computed as the Fourier transform of the transition dipole moment autocorrelation function (computed exactly under the harmonic approximation[55,59]), avoiding any sum-over-states expression.

Under the approximations outlined above, the vibronic spectra can be computed using the transition dipole moments, the harmonic frequencies of the electronic states involved in the process and the so-called Duschinsky transformation[60]. This is an affine transformation between the normal modes of the initial ($\bar{Q}$) and final ($\bar{\bar{Q}}$) states and is reported in the following:

$$\bar{\mathbf{Q}} = \mathbf{J}\bar{\bar{\mathbf{Q}}} + \mathbf{K} \quad (1)$$

where **J** and **K** are usually referred to as Duschinsky matrix and shift vector. The **J** matrix takes into account the modification of the Potential Energy Surface (PES) that occurs with the electronic transition. Instead, the **K** vector describes the change of the nuclear equilibrium position along each normal mode moving from a PES to another. Different expressions for **J** and **K** are obtained depending on the reference geometry used in the harmonic expansion of the final state PES.[52,54]

In the Adiabatic Hessian (AH) model, the final state PES is expanded about its minimum, The calculation of **J** requires the knowledge of the harmonic frequencies of electronic excited states, which is usually the most expensive step of the whole simulation. Approximated models, referred to as Adiabatic Shift (AS), can be obtained by assuming that ES normal modes and harmonic frequencies are the same of the GS and expanding the finale state PES respectively around the its minimum and the equilibrium position of the initial state PES.

The harmonic approximation of the PESs involved in the electronic transition limits the range of applicability of the models described to semi-rigid systems. For floppy systems, undergoing large-amplitude deformations upon electronic excitation, more refined schemes need to be devised. However, the development of anharmonic vibronic models is not trivial: even if the simplest LAMs (such as torsions and inversions) can be in most cases associated to one mode of an electronic state, this mode is in general coupled to more than a single normal coordinate of the other electronic state. As discussed by some of us,[61,62] if normal modes are computed with Cartesian coordinates as basis set, large, unphysical couplings between low- and high-frequency modes are usually present also for the simplest LAMs and for this reason a full-dimensional anharmonic treatment is usually mandatory[63,64].

A more effective solution is offered by the use of internal coordinates at the harmonic level. It is well known that harmonic frequencies and normal modes do not depend on the coordinate system when they are computed at the equilibrium position of a single electronic state. However, for vibronic spectroscopy, which involves more than one PES, the definition of **J** and **K** changes if either cartesian or internal coordinates are employed[61,62,65–68]. When LAMs are present, the coupling between modes is usually strongly reduced if internal coordinates are employed and this improves the reliability of the simulations already at the harmonic level[27,38].

These refined computational tools allows to define a protocol able to describe accurately ground and excited state PESs and the relative electronic transition, also effectively taking into account thermal and solvent contributions, that strongly influence the vibronic progression. As will be demonstrated in the following, the interplay between solvent influence and nuclear rearrangements in both the states involved in the electronic transition has a huge impact on the spectroscopic observables of the large and floppy chemical system under study.

Computational Details

The ground state properties were obtained with DFT (B3LYP[69,70] and CAM-B3LYP[71] functionals) methods, while the excited state investigation was performed with TD-DFT (B3LYP, CAM-B3LYP functionals). Vibrational frequencies were determined for each state, to assure the structures to correspond to potential energy surface minima (absence of imaginary frequencies). No symmetry constrains were applied to reduce the computational effort. The 6-31+G* basis set was selected to carry out all calculations, according to previous literature[10].

Vibronic TI simulations were performed using the standard parameters for the pre-screening scheme, and in all cases a convergence >90% was reached. TD calculations were performed using a total time propagation of 10^{-11} s and a grid of integration with 2^{18} points. Delocalized internal coordinates (DICs)[61,72] were used as set of non-redundant internal coordinates, which are defined univocally starting from the molecular topology. Out-of-plane coordinates were added to each planar, tri-coordinated center.

Bulk solvent effects were systematically accounted for by using the PCM[47]. A static dielectric constant $\varepsilon = 35.6880$ and an optical dielectric constant $\varepsilon_\infty = 1.8069$ were employed for the acetonitrile (MeCN) solvent. Nonelectrostatic terms were included in the evaluation of the relative stability of the different ground state conformers by using the SMD parametrization[73]. All vertical transition energies were computed within the solvent nonequilibrium regime[51], while excited state optimizations and frequency calculations were performed by considering the solvent to be fully equilibrated with the excited state wavefunction.

Atoms In Molecules (AIM) computations were carried out with the AIMPAC[74,75] set of programs, for atomic properties and the electron density critical points. First and second derivatives of the electron density were determined with the use of the PROAIM[74] program. The same set of programs was employed to calculate atomic overlap matrices as well as atomic electronic populations. All the quantum-mechanical calculations were performed using a locally modified version of the Gaussian package[76].

Results and Discussion

Ground State Characterization

The first step of the computational protocol involves the characterization of the GS most stable conformers for both the isolated molecule (gas-phase) and the solvated system in acetonitrile solution. Such an analysis permits to identify four conformers, with different orientation of the thiophene rings with respect to each other and with the quinolinium ring (Fig. 2).

Fig. 2 Most stable geometries of conformers, obtained with B3LYP in vacuum, using the 6-31+G* basis set.

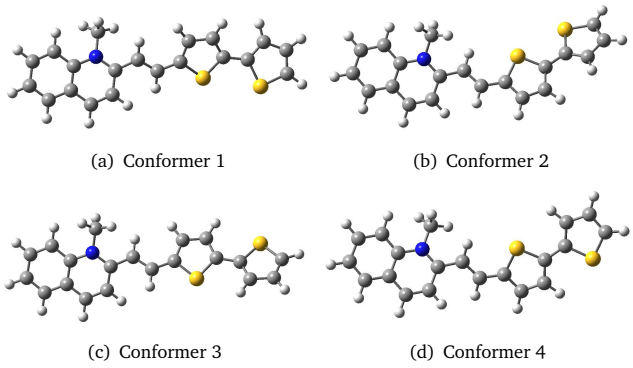

(a) Conformer 1 (b) Conformer 2

(c) Conformer 3 (d) Conformer 4

The relative stability of the equilibrium structures reported in Fig. 2 in terms of Boltzmann populations at room temperature (298 K) is shown in Table 1. The reported data refer to B3LYP calculations in vacuum and MeCN, and include Zero-Point Vibrational Energy (ZPVE), thermal corrections (calculated within the harmonic approximation), and nonelectrostatic energy contributions in case of PCM values.

Table 1 B3LYP/-31+G* Boltzmann populations (in percentage) of stable conformers in vacuo and MeCN.

	Conformer 1	Conformer 2	Conformer 3	Conformer 4
Vacuum	2.0	28.5	7.0	62.5
MeCN	4.9	24.9	1.6	68.5

The data in Table 1 clearly show that conformers 2 and 4 contribute to more than 90% of the total population. Solvent effects affect the population analysis by nearly 5%, however, the prevalence of conformer 4 is confirmed. Therefore, for the sake of brevity, most of the results presented in the following two sections refer to conformer 4 only, while all conformers are considered for comparisons with experimental spectra. The complete data set for all conformers is given as Electronic Supplementary Information (ESI).

Two parameters have been chosen in order to characterize GS structures: the Bond Length Alternation (BLA) and the Delocalization Index Alternation (DIA).

The Bond Length Alternation (BLA) is a geometrical parameter calculated as the difference between the mean length of single bonds and multiple bonds in a π-delocalized subsystems. The BLA systematically decreases when the chain lengthens, as a result of the improved delocalization of the π-electrons, i.e. the more the bonds are delocalized, the less the BLA is[77–79]. When the donor and acceptor groups are weak, the molecule has a structure with a distinct alternation in the bond length among neighboring carbon atoms, which means a high value of BLA. As donor and acceptor substituents become stronger, the contribution of ionic resonance forms to the ground state increases, and BLA first decreases toward zero (partial charge separation), then increases again to high, negative, values (full charge separation: zwitterionic form). The relative contribution of these three resonance forms to the GS is also controlled by the polarity of the solvent where the chromophore is dissolved[80]. Therefore, the BLA provides direct information about equilibrium nuclear distances in the evaluated electronic state and also indirect data, both concerning the resonance form (neutral or zwitterionic) which dominates the GS of a conjugated push-pull system and the electronic delocalization along the π-chain.

Complementary information is obtained through an Atoms In Molecules (AIM) analysis[81], which provides a solid method to separate a molecule into its constituent atoms, considering the Delocalization Index (DI) of bonds $\delta(A,B)$[82,83]. This is a numerical parameter able to quantify the bond strength between two atoms, reflecting the number of electrons shared between them. At the single determinant level of theory, the delocalization index can be calculated from the following expression[84]:

$$\delta(A,B) = -2\sum_{i,j} S_{ij}(A)S_{ij}(B) \qquad (2)$$

where $S_{ij}(A)$ is the overlap of the occupied molecular orbitals i and j within the basin of atom A, the latter defined as the regions in real space enclosed by a zero-flux density surface, or by infinity. The DI analysis is particularly interesting if used to describe the level of delocalization of electrons through the computation of what we have called DIA. We define the DIA as the modulus of the difference of single and multiple bond DI mean values. It gives a direct insight about the modification of the electronic distribution along a conjugated chain when the environment changes, e.g. moving from vacuum to a polar solvent. Indeed, the larger is the difference of bond strengths in the π-chain, the less is the delocalization of the electrons.

In Table 2, BLA and DIA values obtained with two different functionals, B3LYP and CAM-B3LYP, in vacuum and acetonitrile, are reported for the most stable conformer 4. Data refer to the π-chain of carbon atoms, including the nitrogen (see ESI for more details). The vacuum analysis permits to define reference values only depending on the adopted QM method.

Table 2 B3LYP and CAM-B3LYP BLA (Å) and DIA values for conformer 4 in vacuo and MeCN.

	BLA		DIA	
	B3LYP	CAM-B3LYP	B3LYP	CAM-B3LYP
Vacuum	0.035	0.053	0.11	0.19
MeCN	0.049	0.070	0.18	0.24
Relative Variation	+40 %	+32 %	+64 %	+26 %

Concerning the BLA values, the results are higher for CAM-B3LYP, probably due to the greater zwitterionic character of

the GS structure as increasing the Hatree-Fock exact exchange contribution at long distances[71]. Overall, the electronic picture resulting for BLA analysis is a structure showing an intermediate delocalization of electrons along the conjugated system, due to a partial charge transfer from the sulfur atoms (donors) to the nitrogen (acceptor).

For both electronic descriptions, the inclusion of solvent effects causes the increase of BLA of 30-40%, showing that, as expected, a sensitive modification occurs moving from gas phase to a polar solvent such as acetonitrile. Therefore, equilibrium nuclear positions rearrange significantly under the influence of the solvent, which tends to stabilize a ionic resonance form of the GS where the difference of single and double bond lengths is sharpened.

A complementary description of the conjugation can be extracted from DIA values: CAM-B3LYP ascribes a greater weight to the charge transfer and less delocalized resonance form, while B3LYP, with a less absolute value of DIA, provides a molecular picture where a major conjugation is found in the π-chain. Furthermore, the relative variation, obtained moving from vacuum to MeCN, confirms the insights suggested from BLA: the presence of a polar solvent induces structural modifications in the molecule, towards a more localized electronic density. Therefore, in MeCN the conjugated carbon chain partially loses the delocalization, with a higher distinction of single and double bonds.

Excited State Characterization

In order to investigate the role of different effects on the calculation of OPA spectra is of fundamental importance the evaluation of the nature and relative position of ES potential energy surface with respect to the GS.

The CT nature of the first electronic transition is confirmed by TD-DFT calculations. The orbital approximation allows to visualize the regions involved in the process: it is essentially a HOMO-LUMO transition from the thiophene rings to the quinolinium moiety. In Fig. 3 the difference of the HOMO and LUMO electronic densities, obtained at CAM-B3LYP level of theory in acetonitrile, using the 6-31+G* basis set, is sketched.

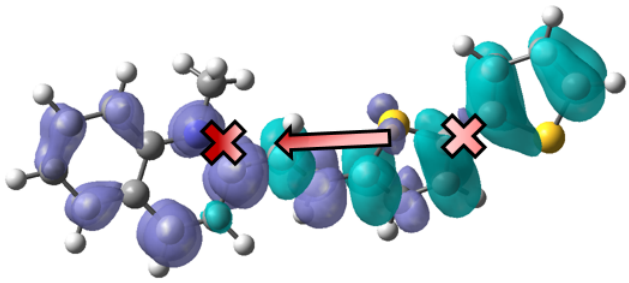

Fig. 3 Conformer 4 HOMO (light blue) and LUMO (blue) orbital electron densities difference, obtained from CAM-B3LYP/6-31+G* TD-DFT calculation in MeCN.

To quantify the extension of the length and magnitude of the electron transfer, a simple and intuitive index recently developed has been used[85]. It is based on the definition of the barycenters of the positive and negative density distributions, obtained from the difference of the total densities of GS and ES. The CT length (D_{CT}) is chosen as the distance between the two barycenters. Moreover, using the same positive and negative density distributions it is possible to define the transferred charge and, therefore, the variation of the dipole moment between the ground and the excited states (μ_{CT}). This couple of parameters allow to quantify both the extension and the magnitude of the charge transfer involved in the electronic transition. The computed D_{CT} and μ_{CT} for the two functional B3LYP and CAM-B3LYP, in vacuo and acetonitrile, are reported in Table 3 for the conformer 4 (see supporting info for the others).

Table 3 B3LYP and CAM-B3LYP D_{CT} (Å) and μ_{CT} (Debey) values for conformer 4 in vacuo and MeCN.

	B3LYP		CAM-B3LYP	
	D_{CT}	μ_{CT}	D_{CT}	μ_{CT}
Vacuum	2.895	6.028	3.042	7.928
MeCN	4.377	11.882	3.829	11.966
Relative Variation	+51%	+97%	+26%	+51%

The large values of D_{CT} in Table 3 confirm the CT character of the electronic transition in all the examined cases. As expected, both B3LYP and CAM-B3LYP report an increase of μ_{CT} (i.e. the magnitude of the CT) in presence of the solvent. Moreover, the calculated relative variations are in agreement with trend reported above for the two functionals, with B3LYP more sensitive to the environment than CAM-B3LYP.

Since the CT nature of the first electronic transition, the choice of the proper exchange-correlation functional to perform the ES investigation within the TD-DFT framework becomes crucial[39–41,86]. In the literature several functionals have been proposed in order to properly describe CT transitions[87–89]. Among them the CAM-B3LYP functional has been chosen in the present work[10,18,19].

The most easily accessible and mainly used parameter to quantify the energy gap between two PESs involved in an absorption process and to evaluate the performances of theoretical approaches is the VT[1–8]. This is defined as the energy difference of the two PESs calculated at the equilibrium geometry of the initial electronic state. The VT is directly associated with the intuitive representation, given from the FC approximation, of an electronic transition that takes place in a timescale faster than characteristic time of nuclear motions, where nuclei are left frozen at initial positions.

As expected for a CT transition, a deep disagreement between global hybrid and range-separated functionals VTs is found, as reported in Table 4, where VT (B3LYP and CAM-B3LYP) and 0-0 predictions (CAM-B3LYP) in vacuo and acetonitrile are reported, obtained for the most stable conformer 4 with the 6-31+G* basis set (further information about the VTs for the other stable conformers can be found in ESI).

For both the approaches, the inclusion of the solvent appears to be of great importance, changing the position of the VT from +42 nm (B3LYP) to -15 nm (CAM-B3LYP). Concerning the density functional choice, the increase of the exact HF exchange in the

Table 4 B3LYP and CAM-B3LYP VT and 0-0 transition energies (nm) for conformer 4 in vacuo and MeCN (basis set: 6-31+G*).

	B3LYP	CAM-B3LYP	
	VT	VT	0-0
Vacuum	537	470	480
MeCN	576	455	521

long-range region of CAM-B3LYP has an impressive effect, shifting the band, with respect to B3LYP, by more than 120 nm. It highlights the importance of the knowledge of the electronic transition nature either from experimental data (strong solvatochromic effect) or theoretical characterizations. On the basis of these results, since only CAM-B3LYP describes the hypsocromic effect of the solvent, this functional has been chosen to carry out the ES investigation and, particularly, the solvent influence on the energy gap of the electronic transition.

In addition to the VT, the energy separation between two electronic state has been characterized with the 0-0 transition, corresponding to the absolute energy difference between the vibrational ground level of ES and GS [10,13,14]. This parameter seems to be more appropriate than VT for those system whose absorption spectrum exhibits a short, structureless vibronic progression.

Nevertheless, unexpected effects of the solvent are reported: moving from the gas phase to acetonitrile, the VT exhibits a blue-shift, while the 0-0 is shifted to the red region. Therefore, the consequences of the solvent presence cannot be described as a simple modification of the energy gap between the PESs involved in the absorption process, as will be highlighted in the following section.

One Photon Absorption Spectra

In this section we will focus on the description of the OPA spectrum, dissecting the different physico-chemical contributions to the bandshape. The main terms that modify the absorption spectral profile are the vibronic progression, solvent effects, thermal contributions and conformational weights. Our computational protocol allows to include all these terms with a step-by-step procedure, so as to separate and identify their role on the final bandshape.

As highlighted above, the use of CAM-B3LYP for the investigation of the ES is mandatory, while for the description of the starting electronic state frequencies B3LYP functional has been used, due to its well known good performances in the GS characterization [90,91]. All spectra reported have been obtained following this protocol. Moreover, in almost all the cases the Adiabatic Hessian (AH) approach has been employed using internal coordinates [38,62], which permits to deal with a medium-to-large flexible system that, otherwise, would not be possible to treat with high level vibronic models.

The starting point for a proper characterization of an OPA spectrum is the inclusion of the vibronic progression for a single conformer (the most stable 4) in vacuum at 0 K temperature. In this way, solvent, temperature and conformational weights are neglected. In ESI, additional data for all the conformers (Fig. S2) and the comparison between the computation of Time-Independent (TI) and Time-Dependent (TD) vibronic spectra (Fig. S3) are presented.

Fig. 4 reports the comparison between TD|AH vibronic spectra in vacuo and MeCN at 0 K for conformer 4. The two spectra have been shifted for the 0-0 transition energy evaluated in MeCN, in order to highlight solvent effects on the spectral profile and the band position. From TI analysis in vacuo, normal modes corresponding to an overall distortion of the molecules are found to be active (their graphical representation is given in ESI, Fig. S4). The low frequency values of the active normal modes is coherent with the narrow vibronic progression of the spectrum, corresponding to small displacements of the ES PES along these normal coordinates. Therefore, the tight progression is representative of a minor modification of the equilibrium position of the ES with respect to the GS (small components of the **K** shift vector).

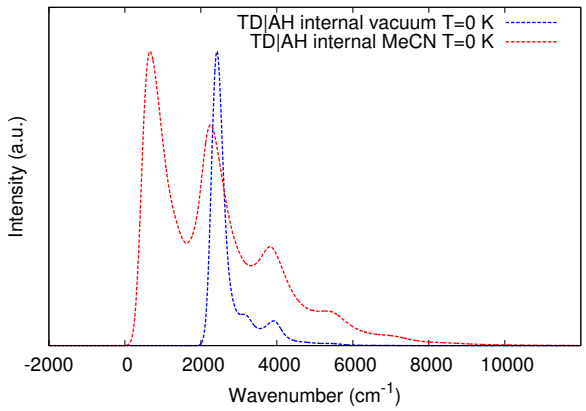

Fig. 4 Comparison of TD|AH vibronic spectra (T=0 K) in vacuo and MeCN. Calculations were performed in internal coordinates by using B3LYP (GS frequencies) and CAM-B3LYP (0-0 energy and ES frequencies). The zero reference value for the energy is set to the 0-0 transition energy evaluated in MeCN. Data refer to conformer 4.

Interestingly, the modification of the bandshape due to the solvent effect is found to be substantial. The vibronic progression broadens of some thousands of wavenumbers, the position is red-shifted of nearly 2000 cm^{-1} and a clear regular progression emerges at multiple of nearly 1500 cm^{-1}. The presence of such an extended vibronic progression is associated with a large displacement of the relative position of the two PESs along the high frequency normal coordinate.

The superposition of GS and ES optimized geometries, reported in Fig. 5, shows a large displacement of dihedral angles of thiophene rings, however these modifications are associated with low frequency tilt motions, that cannot justify such a broad spectral progression.

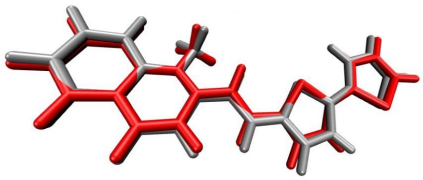

Fig. 5 Comparison of GS (red) and ES (silver) optimized geometries at CAM-B3LYP/6-31+G* level in MeCN for conformer 4.

Indeed, the large mobility of thiophene rings is due to the small energy barriers that separate the four conformers in the GS and this kind of active normal modes can be safely associated with the broadening of each peak of the sharp vibronic progression.
In order to identify high frequency active normal modes, it is possible to separate the two main effects that contribute to the vibronic spectrum: the variation in the equilibrium position of the PESs involved in the electronic transition (described by the shift vector **K** and responsible for the extension of the progression) and the change of the PES shape that accompanies the transition from the GS to the ES (taken into account by the Duschinsky matrix **J**). This can be done by adopting the Adiabatic Shift (AS) vibronic model, which takes into account the effect of **K** only. In Fig. 6 the comparison between the TD|AH vibronic spectrum and both the TI|AS stick and TI|AS broadened spectra of conformer 4 in MeCN at T=0 K are reported.

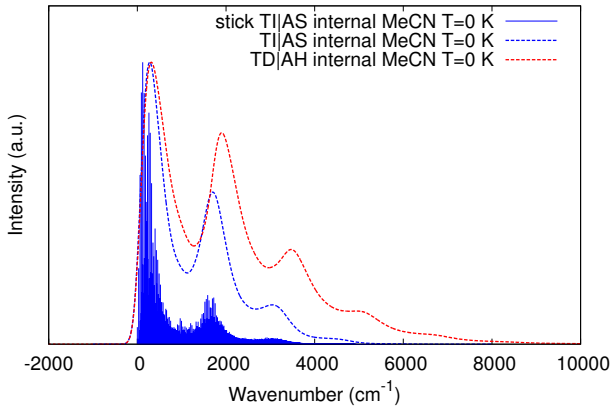

Fig. 6 Comparison of stick and convoluted TI|AS spectra with TD|AH vibronic spectra, at T=0 K in MeCN. Calculations were performed by using B3LYP (GS frequencies) and CAM-B3LYP (0-0 energy and ES frequencies). The zero reference value for the energy is set to the 0-0 transition energy calculated in MeCN. Data refer to conformer 4.

Fig. 6 shows that the AH vibronic progression is well reproduced by the AS model. The use of the TI approach allows to assign each transition to the corresponding vibrational level of the ES: the spectral progression is attributed to a single high frequency normal mode (81) at 1426.74 cm^{-1}, involved in combination bands with low frequency modes. The overall displacement associated with this particular coordinate is sketched in Fig. 7 for conformer 4.

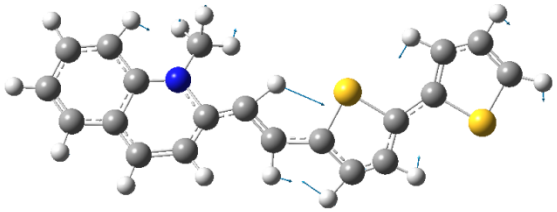

Fig. 7 Pictorial view of the 1426.74 cm^{-1} active normal mode (81th) involved in the absorption process. B3LYP/6-31+G* in MeCN for conformer 4.

Remarkably, the active normal mode corresponds to the modification of nuclear positions reported in the discussion of the BLA section. Indeed, it was shown that the solvent presence stabilizes a ionic resonance form, where part of the delocalization is lost. The partial charge transfer, due to the polarity of the solvent and occurring from the thiophene moieties to the quinolinium ring, is accompanied with a variation of the equilibrium positions toward a configuration where a sharper alternation in the bond length among neighboring carbon atoms is present. Therefore, it is not surprising that a similar reorganization happens in acetonitrile moving from the GS to ES, which has a well defined charge transfer character, as already pointed out by the Charge-Transfer indexes reported in Table 3.
As stated before, the extension of a vibronic progression is due to large displacements of the PESs along one or more normal coordinates. Therefore, the pattern found in the vibronic spectrum can be easily interpreted within the FC framework at the harmonic level: the maximum overlap between the GS and ES vibrational eigenfunctions, evaluated at the equilibrium geometry of the GS, is obtained with the first low levels of the 81th normal mode, leading to equally spaced intense peaks over an overall range of nearly 8000 cm^{-1}.
The elucidation given through the vibronic analysis allows to understand the different behavior of the molecule in vacuum and in MeCN and to clarify the results obtained for VT and 0-0 transitions. In Fig. 8 the expected energy scheme of the absorption spectrum is illustrated in gas phase and in polar solvent.

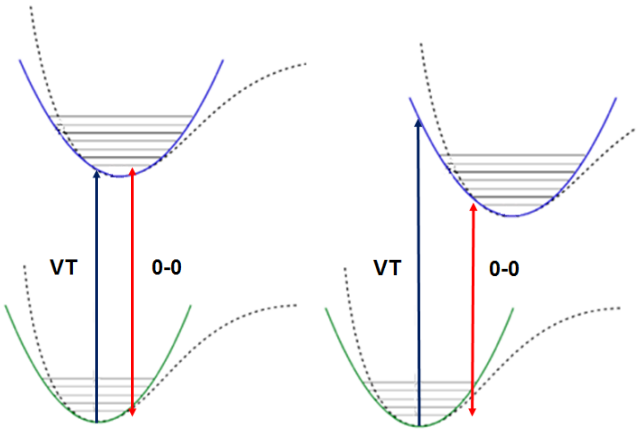

(a) vacuum (b) MeCN

Fig. 8 Pictorial view of the PESs along the 81th normal coordinate, in vacuo (left) and MeCN (right).

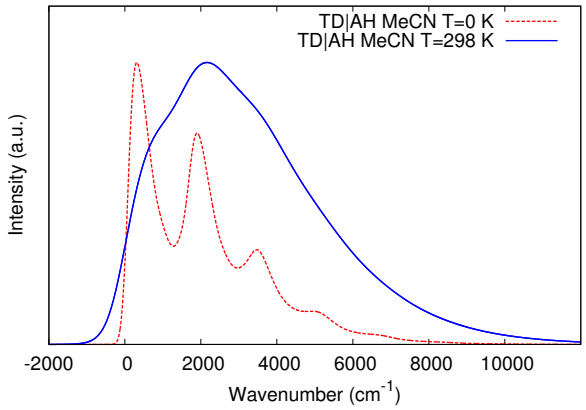

Fig. 9 Comparison of TD|AH vibronic spectra at 0 and 298 K in MeCN. B3LYP (GS frequencies) and CAM-B3LYP (0-0 energy and ES frequencies) are used. Both spectra are shifted for the 0-0 transition energy in MeCN. Data refer to conformer 4.

The main effect of the solvent is to stabilize charge transfer forms, both in the GS and in the ES. Given the charge transfer nature of the HOMO-LUMO transition involved in the absorption process, a stronger effect on the ES is expected. Therefore, as illustrated in Fig. 8, the equilibrium position of the ES is simultaneously strongly stabilized and shifted along the normal coordinate corresponding to a rearrangement of nuclear positions of the π-chain, in a way similar to that illustrated in the BLA discussion. As a consequence, the 0-0 transition is red-shifted from 480 (gas phase) to 521 nm (acetonitrile), while the VT, involving high frequency excited vibrational levels of the ES, is blue-shifted from 470 (gas phase) to 455 nm (acetonitrile).

Such an analysis sheds light on the intriguing behavior of such class of push-pull system, exhibiting an hypsochromic behavior despite the charge transfer nature of the first ES. This interpretation allows to propose a grounded explanation of the experimentally observed negative solvatochromism, demonstrating the substantial modification of nuclear positions during the electronic excitation.

The data reported so far refer to 0 K, however in order to get a reliable description of experimental finding, temperature effects have to be considered. In TD vibronic models the reference temperature can be straightforwardly chosen without any additional computational effort[55]. By setting a reference temperature different from 0 K, the Boltzmann populations of harmonic vibrational levels of the GS are considered. Therefore, the absorption spectrum results as the sum of all the possible transitions from accessible GS vibrational levels to those of the ES. The predictions of such calculations are shown in Fig. 9, where the comparison between TD|AH vibronic spectra in internal coordinates, obtained in acetonitrile at 0 and 298 K for conformer 4, is reported. As before, the zero reference value for the energy is set to the 0-0 transition energy.

The inclusion of thermal contributions provides an inhomogeneous broadening of each peak of the progression, due to the fact that several low-lying initial vibrational levels become accessible at room temperature. As a consequence, despite the use of the same phenomenological Gaussian distribution function, with HWHM of 135 cm^1, an increasing of the band width is obtained at 298 K. Moreover, a clear increase of the intensity of excited level peaks is shown, shifting the maximum of the band to the blue, far from the 0-0 transition value. The shifted spectrum reported in Fig. 9 underlines the small correction due to the temperature for negative wavenumbers. This is the fingerprint of contributions of the excited vibrational levels of the GS. Indeed, only vibronic transitions starting from excited GS levels and arriving to low-lying ES vibrational levels can give an energy gap smaller than the 0-0 transition. The resulting spectral profile modification is extremely important, since it highlights the necessity of the inclusion of thermal effects in the vibronic calculations and underlines that the maximum of the OPA spectrum cannot be associated a-priori with simple parameters such as the VT or the 0-0 transition.

Comparison Between Theory and Experiment

In order to highlight the role of the effects described above, in this section each contribution is included step-by-step and the resulting spectra are compared with the experiment.

In ESI (Fig. S5) the comparisons between the normalized experimental spectrum and VTs computed for the four conformers (weighted for their Boltzmann factor evaluated at 298 K) are reported in vacuo and MeCN. The agreement between VTs and the band maximum is only deceptive and due to a compensation of effects. Indeed, the correspondence with the experiment is worse in solution than in vacuo.

In Fig. 10 the comparison between the experiment in MeCN and the vibronic spectra computed in vacuo and MeCN at 0 Kelvin are reported. The TD|AH approach has been employed, and all the four most stable conformers have been considered, scaled for their Boltzmann populations.

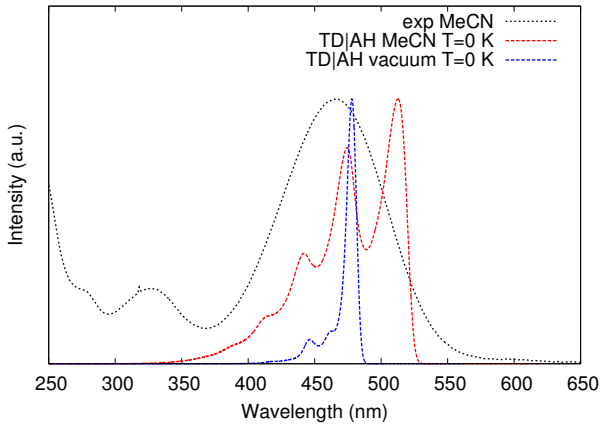

Fig. 10 Comparison between the normalized experimental spectrum in MeCN and TD|AH spectra computed in internal coordinates at 0 K in vacuo and MeCN. B3LYP (GS frequencies) and CAM-B3LYP (0-0 energy and ES frequencies) are used. The four most stable conformers have been taken into account, scaled by their Boltzmann populations.

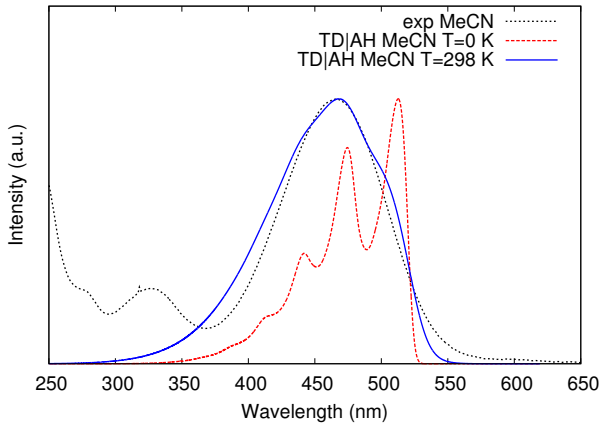

Fig. 11 Comparison between the normalized experimental spectrum in MeCN and TD|AH spectra computed in internal coordinates at 0K and 298K in MeCN. B3LYP (GS frequencies) and CAM-B3LYP (0-0 energy and ES frequencies) are used. The four most stable conformers have been taken into account, scaled by their Boltzmann populations.

The experiment shows a broad band in the long wavelength region, well separated from the others and safely assigned to the first electronic transition, with the maximum centered at 466 nm and Full Width at Half Maximum (FWHM) of nearly 90 nm (4000 cm^{-1}). The shape of the experimental spectrum is typical for a medium-to-large flexible molecule in condensed phase at room temperature, where low frequency accessible vibrational levels cause the band broadening and the solvent is responsible for the observed inhomogeneous broadening, due to several possible configurations of the solute-solvent couple.

As expected, the spectrum at 0 K for the isolated molecule badly reproduces the experimental maximum and bandshape. The comparison is improved by considering the presence of the solvent; in fact, by even using the same phenomenological narrow distribution function (Gaussian with HWHM of 135 cm^{-1}), the band progression becomes extremely wider, with an extension comparable to the experiment. Interestingly, even in presence of an intense vibronic progression, the maximum of the spectrum moves in the red region, close to the 0-0 transition.

A further step to refine the comparison between calculations and the experiment requires to include temperature effects. The results are reported in Fig. 11.

The exceptional agreement has been obtained adopting the TD approach in internal coordinates (AH model), including the contributions of the four stable conformer, weighted for their Boltzmann factors at room temperature. Substantial modification are introduced taking into account thermal contributions. The expected broadening and the red shift of the maximum of intensity correct the band profile and increase the overlap with the experiment. Indeed, the shape and the width of the curve are very well reproduced, even with the inclusion of narrow distribution functions (Gaussians with HWHM of 135 cm^{-1} have been employed), and the band position is quite exact, with an error of only 2 nm. Such an impressive agreement is due to application of reliable methodologies for each part of the calculation (particularly, for the GS frequencies and both the energy gap and the ES properties).

The slight overestimation of the band broadening and the differences at long wavelengths can be explained taking into account the less precise reproduction of low-frequency force constants at the harmonic level. Therefore, improvements are expected by moving to an anharmonic treatment of these normal modes[53,55,63,92–95], especially with the inclusion of vibrational nonequilibrium effects in the frequency calculation[96–99].

It is worth stressing that the excellent agreement between theory and experiment has been obtained only by including in the computation the fundamental physico-chemical contributions affecting the spectral shape/position. Indeed, simplified approaches, relying on VTs ot 0-0 transitions are unable to reproduce the experimental maximum intensity wavelength at this level of accuracy. This is further shown in Table 5, where experimental and theoretical (vibronic spectrum in MeCN at 298 K) maxima are collected together with the mean of both VT and 0-0 transition, obtained taking into account the four stable conformers weighted for their relative stability in MeCN at room temperature.

Relative to the experiment, the errors are +2, -14 and +53 nm for the maximum of the vibronic spectrum, the VT and the 0-0 transition, respectively. Interestingly, had the reported results

Table 5 Intensity maxima (nm) of the experimental and theoretical vibronic spectra (in MeCN at 298 K, including all the four most stable conformers). Conformatonally weighted VTs and 0-0 transitions (in MeCN) are also reported for the sake's of comparison.

Experiment	466
Computed spectrum	468
Weighted VT	452
Weighted 0-0	519

been obtained in a benchmark work, the 0-0 value would not have been classified as satisfying, despite the perfect agreement of the vibronic prediction based on it. Moreover, the weighted VT, as previously outlined, agrees quite well only for an error cancellation.

Summary and Conclusions

The influence of different physical contributions on the OPA spectrum have been theoretically investigated for a particularly challenging chemical system, using a novel refined internal coordinates vibronic approach, which gives the possibility to properly describe floppy chemical systems strongly sensitive to solvent. A separate and detailed analysis of each od the terms affecting the spectrum has been performed, allowing to get valuable insights, hidden beyond the broad electronic spectrum. Such an analysis would not have been possible based on the low-resolution experimental spectrum alone.

The fundamental role of the solvent on the vibronic progression has been underlined. A theoretical interpretation has been proposed in order to clarify the apparent discrepancies between the VT and the 0-0 predictions, which are at the origin of the exhibited hypsochromic behavior of the molecule.

Indeed, the rearrangement of nuclear equilibrium positions in the presence of the solvent, already noticed in the GS through the BLA and DIA analysis, has been observed to be associated, even more sharpened, to the electronic transition process. The electronic excitation implies a remarkable shift of the ES PES along high frequency normal modes. This strongly stabilizes the ES equilibrium position but also increases the vertical gap between the PESs involved. Therefore, the more intense is the solvent effect (associated with the polarity of the solvent), the more marked are the red-shift of the 0-0 transition and the blue-shift of the VT.

Furthermore, this study highlights the critical modifications of the spectral profile associated with thermal contributions. Especially for large, flexible systems, where the correction to the VT and 0-0 transition are supposed to be relevant, a poor evaluation of the OPA maxima can provide misleading results about the quality of the DFT functional. Conversely, the exceptional agreement between the experiment and the theoretical prediction obtained in this work strongly suggests the importance of going beyond the oversimplified comparison between experimental absorption maxima and computed VT or 0-0 transitions. Only a complete description of all the contributions that can influence the absorption spectrum is trustworthy, and permits to gain most of the rich information enclosed into the molecular spectrum.

Acknowledgments

Thanks are due to Prof. C.G. Fortuna, University of Catania, for supplying the substrate. BC and FE acknowledge support from the Italian "Ministero per l'Università e la Ricerca Scientifica e Tecnologica", MIUR (Rome, Italy) under the FIRB "Futuro in Ricerca" 2013, no. RBFR13PSB6.

References

1 M. R. Silva-Junior, M. Schreiber, S. P. Sauer and W. Thiel, *J. Chem. Phys.*, 2008, **129**, 104103.
2 D. Jacquemin, E. A. Perpete, G. E. Scuseria, I. Ciofini and C. Adamo, *J. Chem. Theory Comput.*, 2008, **4**, 123–135.
3 S. P. Sauer, M. Schreiber, M. R. Silva-Junior and W. Thiel, *J. Chem. Theory Comput.*, 2009, **5**, 555–564.
4 L. Goerigk, J. Moellmann and S. Grimme, *Phys. Chem. Chem. Phys.*, 2009, **11**, 4611–4620.
5 M. R. Silva-Junior, S. P. Sauer, M. Schreiber and W. Thiel, *Mol. Phys.*, 2010, **108**, 453–465.
6 D. Jacquemin, E. A. Perpète, I. Ciofini and C. Adamo, *Theo. Chem. Acc.*, 2011, **128**, 127–136.
7 S. S. Leang, F. Zahariev and M. S. Gordon, *J. Chem. Phys.*, 2012, **136**, 104101.
8 C. A. Guido, D. Jacquemin, C. Adamo and B. Mennucci, *J. Phys. Chem. A*, 2010, **114**, 13402–13410.
9 L. Goerigk and S. Grimme, *J. Chem. Phys.*, 2010, **132**, 184103.
10 D. Jacquemin, A. Planchat, C. Adamo and B. Mennucci, *J. Chem. Theory Comput.*, 2012, **8**, 2359–2372.
11 N. O. Winter, N. K. Graf, S. Leutwyler and C. Hättig, *Phys. Chem. Chem. Phys.*, 2013, **15**, 6623–6630.
12 C. Fang, B. Oruganti and B. Durbeej, *J. Phys. Chem. A*, 2014, **118**, 4157–4171.
13 D. Jacquemin, I. Duchemin and X. Blase, *J. Chem. Theory Comput.*, 2015, **11**, 5340–5359.
14 D. Jacquemin, B. Moore, A. Planchat, C. Adamo and J. Autschbach, *J. Chem. Theory Comput.*, 2014, **10**, 1677–1685.
15 M. Dierksen and S. Grimme, *J. Phys. Chem. A*, 2004, **108**, 10225–10237.
16 A. Charaf-Eddin, A. Planchat, B. Mennucci, C. Adamo and D. Jacquemin, *J. Chem. Theory Comput.*, 2013, **9**, 2749–2760.
17 B. Moore, A. Charaf-Eddin, A. Planchat, C. Adamo, J. Autschbach and D. Jacquemin, *J. Chem. Theory Comput.*, 2014, **10**, 4599–4608.
18 J. Cerezo, F. J. A. Ferrer and F. Santoro, *Phys. Chem. Chem. Phys.*, 2015, **17**, 11401–11411.
19 F. Muniz-Miranda, A. Pedone, G. Battistelli, M. Montalti, J. Bloino and V. Barone, *J. Chem. Theory Comput.*, 2015, **11**, 5371–5384.
20 F. Santoro and D. Jacquemin, *WIRES: Computational Molecular Science*, 2016, **6**, 460–486.
21 D. Jacquemin and C. Adamo, *Density-Functional Methods for Excited States*, Springer, 2015, pp. 347–375.

22 E. Benassi, C. Cappelli, B. Carlotti and V. Barone, *Phys. Chem. Chem. Phys.*, 2014, **16**, 26963–26973.

23 T. Hede, N. A. Murugan, J. Kongsted, C. Leck and H. Ågren, *J. Phys. Chem. A*, 2014, **118**, 1879–1886.

24 C. A. Guido, S. Knecht, J. Kongsted and B. Mennucci, *J. Chem. Theory Comput.*, 2013, **9**, 2209–2220.

25 M. Hodecker, M. Biczysko, A. Dreuw and V. Barone, *J. Chem. Theory Comput.*, 2016, **12**, 2820–2833.

26 G. Prampolini, F. Bellina, M. Biczysko, C. Cappelli, L. Carta, M. Lessi, A. Pucci, G. Ruggeri and V. Barone, *Chem-Eur. J.*, 2013, **19**, 1996–2004.

27 A. Baiardi, J. Bloino and V. Barone, *J. Chem. Theory Comput.*, 2017.

28 C. G. Fortuna, C. Bonaccorso, F. Qamar, A. Anu, I. Ledoux and G. Musumarra, *Org. Biomol. Chem.*, 2011, **9**, 1608–1613.

29 C. G. Fortuna, V. Barresi and G. Musumarra, *Bioorg. Med. Chem.*, 2010, **18**, 4516–4523.

30 M. Pawlicki, H. A. Collins, R. G. Denning and H. L. Anderson, *Angew. Chem. Int. Ed.*, 2009, **48**, 3244–3266.

31 W. Fisher, W. Partridge, C. Dees and E. Wachter, *Photochem. Photobiol.*, 1997, **66**, 141–155.

32 W. R. Zipfel, R. M. Williams and W. W. Webb, *Nat. Biotechnol.*, 2003, **21**, 1369–1377.

33 G. C. Ellis-Davies, *Nat. Methods*, 2007, **4**, 619–628.

34 B. Carlotti, G. Consiglio, F. Elisei, C. G. Fortuna, U. Mazzucato and A. Spalletti, *J. Phys. Chem. A*, 2014, **118**, 3580–3592.

35 B. Carlotti, E. Benassi, V. Barone, G. Consiglio, F. Elisei, A. Mazzoli and A. Spalletti, *ChemPhysChem*, 2015, **16**, 1440–1450.

36 B. Carlotti, E. Benassi, C. G. Fortuna, V. Barone, A. Spalletti and F. Elisei, *ChemPhysChem*, 2016, **17**, 136–146.

37 S. Caldarelli, D. Catalano, L. Di Bari, M. Lumetti, M. Ciofalo and C. A. Veracini, *J. Mol. Struct.*, 1994, **323**, 181–191.

38 J. Bloino, A. Baiardi and M. Biczysko, *Int. J. Quantum Chem.*, 2016, **116**, 1543–1574.

39 A. Dreuw and M. Head-Gordon, *J. Am. Chem. Soc.*, 2004, **126**, 4007–4016.

40 P. Wiggins, J. G. Williams and D. J. Tozer, *J. Chem. Phys.*, 2009, **131**, 091101.

41 A. D. Laurent and D. Jacquemin, *Int. J. Quantum Chem.*, 2013, **113**, 2019–2039.

42 A. Warshel and M. Levitt, *J. Mol. Biol.*, 1976, **103**, 227–249.

43 A. Warshel and M. Karplus, *J. Am. Chem. Soc.*, 1972, **94**, 5612–5625.

44 H. M. Senn and W. Thiel, *Angew. Chem. Int. Ed.*, 2009, **48**, 1198–1229.

45 B. T. Thole, *Chem. Phys.*, 1981, **59**, 341–350.

46 C. Cappelli, *Int. J. Quantum Chem.*, 2016, **116**, 1532–1542.

47 J. Tomasi, B. Mennucci and R. Cammi, *Chem. Rev.*, 2005, **105**, 2999–3094.

48 F. Lipparini and V. Barone, *J. Chem. Theory Comput.*, 2011, **7**, 3711–3724.

49 V. Barone, I. Carnimeo and G. Scalmani, *J. Chem. Theory Comput.*, 2013, **9**, 2052–2071.

50 R. Cammi, *Molecular Response Functions for the Polarizable Continuum Model*, Springer, 2013, pp. 37–45.

51 B. Mennucci, C. Cappelli, C. A. Guido, R. Cammi and J. Tomasi, *J. Phys. Chem. A*, 2009, **113**, 3009–3020.

52 V. Barone, J. Bloino, M. Biczysko and F. Santoro, *J. Chem. Theory Comput.*, 2009, **5**, 540–554.

53 V. Barone, J. Bloino, C. A. Guido and F. Lipparini, *Chem. Phys. Lett.*, 2010, **496**, 157–161.

54 J. Bloino, M. Biczysko, F. Santoro and V. Barone, *J. Chem. Theory Comput.*, 2010, **6**, 1256–1274.

55 A. Baiardi, J. Bloino and V. Barone, *J. Chem. Theory Comput.*, 2013, **9**, 4097–4115.

56 F. Santoro, R. Improta, A. Lami, J. Bloino and V. Barone, *J. Chem. Phys.*, 2007, **126**, 084509.

57 E. J. Heller, *Acc. Chem. Res.*, 1981, **14**, 368–375.

58 S. Mukamel, S. Abe and R. Islampour, *J. Phys. Chem.*, 1985, **89**, 201–204.

59 A. Baiardi, J. Bloino and V. Barone, *J. Chem. Phys.*, 2014, **141**, 114108.

60 F. Duschinsky, *Acta Phys-Chim. URSS*, 1937, **7**, 551.

61 A. Baiardi, J. Bloino and V. Barone, *J. Chem. Theory Comput.*, 2015, **11**, 3267–3280.

62 A. Baiardi, J. Bloino and V. Barone, *J. Chem. Phys.*, 2016, **144**, 084114.

63 V. Rodriguez-Garcia, K. Yagi, K. Hirao, S. Iwata and S. Hirata, *J. Chem. Phys.*, 2006, **125**, 014109.

64 D. W. Mok, E. P. Lee, F.-t. Chau and J. M. Dyke, *J. Chem. Theory Comput.*, 2009, **5**, 565–579.

65 J. R. Reimers, *J. Chem. Phys.*, 2001, **115**, 9103–9109.

66 J. Cerezo, J. Zuniga, A. Requena, F. J. Ávila Ferrer and F. Santoro, *J. Chem. Theory Comput.*, 2013, **9**, 4947–4958.

67 J. Cerezo and F. Santoro, *J. Chem. Theory Comput.*, 2016, **12**, 4970–4985.

68 A. Capobianco, R. Borrelli, C. Noce and A. Peluso, *Theo. Chem. Acc.*, 2012, **131**, 1181.

69 A. D. Becke, *J. Chem. Phys.*, 1993, **98**, 1372–1377.

70 A. D. Becke, *J. Chem. Phys.*, 1993, **98**, 5648–5652.

71 T. Yanai, D. P. Tew and N. C. Handy, *Chem. Phys. Lett.*, 2004, **393**, 51–57.

72 J. Baker, A. Kessi and B. Delley, *J. Chem. Phys.*, 1996, **105**, 192–212.

73 A. V. Marenich, C. J. Cramer and D. G. Truhlar, *J. Phys. Chem. B*, 2009, **113**, 6378–6396.

74 T. Keith, *Resource access mode: http://aim. tkgristmill. com*.

75 F. W. Biegler-könig, R. F. Bader and T.-H. Tang, *J. Comput. Chem.*, 1982, **3**, 317–328.

76 M. J. Frisch, G. W. Trucks, H. B. Schlegel, G. E. Scuseria, M. A. Robb, J. R. Cheeseman, G. Scalmani, V. Barone, B. Mennucci, G. A. Petersson, H. Nakatsuji, M. Caricato, X. Li, H. P. Hratchian, A. F. Izmaylov, J. Bloino, B. G. Janesko, F. Lipparini, G. Zheng, A. Marenich, J. L. Sonnenberg, W. Liang, M. Hada, M. Ehara, K. Toyota, R. Fukuda,

J. Hasegawa, M. Ishida, T. Nakajima, Y. Honda, O. Kitao, H. Nakai, T. V. K. Throssell, J. Montgomery, Jr., J. E. Peralta, F. Ogliaro, M. Bearpark, J. J. Heyd, E. Brothers, K. N. Kudin, V. N. Staroverov, T. Keith, R. Kobayashi, J. Normand, K. Raghavachari, A. Rendell, J. C. Burant, S. S. Iyengar, J. Tomasi, M. Cossi, N. Rega, J. M. Millam, M. Klene, J. E. Knox, J. B. Cross, V. Bakken, C. Adamo, J. Jaramillo, R. Gomperts, R. E. Stratmann, O. Yazyev, A. J. Austin, R. Cammi, C. Pomelli, J. W. Ochterski, R. L. Martin, K. Morokuma, V. G. Zakrzewski, G. A. Voth, P. Salvador, J. J. Dannenberg, S. Dapprich, P. V. Parandekar, N. J. Mayhall, A. D. Daniels, O. Farkas, J. B. Foresman, J. V. Ortiz, J. Cioslowski, and D. J. Fox, *Gaussian 09 Development Version and Revision I04*, Gaussian Inc. Wallingford CT 2014.

77 J. L. Brédas, *J. Chem. Phys.*, 1985, **82**, 3808–3811.

78 J. Gao and C. Alhambra, *J. Am. Chem. Soc.*, 1997, **119**, 2962–2963.

79 D. Jacquemin and C. Adamo, *J. Chem. Theory Comput.*, 2010, **7**, 369–376.

80 R. Cammi, B. Mennucci and J. Tomasi, *J. Am. Chem. Soc.*, 1998, **120**, 8834–8847.

81 R. Bader, *A Quantum Theory, Clarendon*, 1990.

82 R. F. Bader and M. E. Stephens, *J. Am. Chem. Soc.*, 1975, **97**, 7391–7399.

83 R. F. Bader, A. Streitwieser, A. Neuhaus, K. E. Laidig and P. Speers, *J. Am. Chem. Soc.*, 1996, **118**, 4959–4965.

84 J. Poater, M. Solà, M. Duran and X. Fradera, *J. Phys. Chem. A*, 2001, **105**, 6249–6257.

85 T. Le Bahers, C. Adamo and I. Ciofini, *J. Chem. Theory Comput.*, 2011, **7**, 2498–2506.

86 A. Dreuw and M. Head-Gordon, *Chem. Rev.*, 2005, **105**, 4009–4037.

87 J.-D. Chai and M. Head-Gordon, *Phys. Chem. Chem. Phys.*, 2008, **10**, 6615–6620.

88 Y. Zhao and D. G. Truhlar, *Theo. Chem. Acc.s*, 2008, **120**, 215–241.

89 R. Peverati and D. G. Truhlar, *J. Chem. Phys.*, 2011, **135**, 191102.

90 P. Carbonniere, T. Lucca, C. Pouchan, N. Rega and V. Barone, *J. Comput. Chem.*, 2005, **26**, 384–388.

91 Y. Zhao and D. G. Truhlar, *J. Chem. Theory Comput.*, 2008, **4**, 1849–1868.

92 J. M. Luis, D. M. Bishop and B. Kirtman, *J. Chem. Phys.*, 2004, **120**, 813–822.

93 V. Barone, *J. Chem. Phys.*, 2005, **122**, 014108.

94 J. Bloino and V. Barone, *J. Chem. Phys.*, 2012, **136**, 124108.

95 J. Bloino, M. Biczysko and V. Barone, *J. Chem. Theory Comput.*, 2012, **8**, 1015–1036.

96 C. Cappelli, S. Corni, R. Cammi, B. Mennucci and J. Tomasi, *J. Chem. Phys.*, 2000, **113**, 11270–11279.

97 R. Cammi, C. Cappelli, S. Corni and J. Tomasi, *J. Phys. Chem. A*, 2000, **104**, 9874–9879.

98 C. Cappelli, F. Lipparini, J. Bloino and V. Barone, *J. Chem. Phys.*, 2011, **135**, 104505.

99 F. Egidi, T. Giovannini, M. Piccardo, J. Bloino, C. Cappelli and V. Barone, *J. Chem. Theory Comput.*, 2014, **10**, 2456–2464.